

Acoustic wave focusing by 2.5D graded index lens

Cite as: Appl. Phys. Lett. **119**, 141907 (2021); doi: 10.1063/5.0064246

Submitted: 21 July 2021 · Accepted: 13 September 2021 ·

Published Online: 6 October 2021



View Online



Export Citation



CrossMark

Yuanyan Zhao,^{1,a)}  Sriram Subramanian,²  and Gianluca Memoli¹ 

AFFILIATIONS

¹School of Engineering and Informatics, University of Sussex, Brighton BN1 9RH, United Kingdom

²Department of Computer Science, University College London, London WC1E 6EA, United Kingdom

^{a)}Author to whom correspondence should be addressed: yz467@sussex.ac.uk

ABSTRACT

Three dimensional sound convergence in air underpins applications ranging from localized acoustic experiences to levitation. Most current solutions, however, are challenging to scale-up: they either require complex electronics or intricate geometries. In this paper, we propose a solution based on sonic crystals: an extruded 2D hexagonal lattice array of rigid cylinders with gradient diameters, capable of focusing in 3D emission of a standard loudspeaker at audio frequencies, which we call a 2.5D lens. First, we use finite-element simulations to describe the underpinning theory in terms of the band structure and equifrequency contours. We then describe how we manufactured two lenses, one of which has a focal length smaller than the wavelength, and compare pressure with simulations. Our measurements not only show good agreement with simulations but also highlight how the efficiency of such lenses strongly depends on how the sound is delivered to them.

© 2021 Author(s). All article content, except where otherwise noted, is licensed under a Creative Commons Attribution (CC BY) license (<http://creativecommons.org/licenses/by/4.0/>). <https://doi.org/10.1063/5.0064246>

The focusing of light through a lens is a well-known phenomenon, since the times of the ancient Greeks. Optical lenses are simple devices, typically refraction-based, but underpin precise light delivery in many applications, from vision goggles to special effects. An optical lens is, in fact, characterized by only two parameters: its size perpendicular to the propagation of light rays (“lateral dimension”) and its focal length. In optics, the focusing effect is achieved by a variation of the refraction index along the lateral dimension of the lens. In the 1960s, several researchers attempted to create an acoustic equivalent, but their solutions were either bulky or too fragile. Beam-forming technologies in acoustics focused, therefore, on the use of arrays of multiple transducers.

More recently, metamaterials have opened the path to acoustic lenses of more practical size. Acoustic metamaterials are artificial composite materials designed to control sound with extraordinary approaches such as internal complex structures and the theory of homogenization.^{1–3} In the past 20 years, they have been used to realize different acoustic responses such as doubly negative mass density and bulk modulus,¹ carpet cloaking,^{4,5} acoustic holograms,⁶ and acoustic cloaking.⁷ Several kinds of acoustic metamaterial approaches, inspired by optics, have been used to realize acoustic lenses. The “retrieving method,” for instance, utilizes reflection and transmission coefficients to calculate the effective (acoustic) refractive index of 2D cross-shaped structures and to realize focusing in two dimensions.^{8–10} Jin *et al.*¹¹ used multiple soft porous materials to achieve the desired refractive

index across the lateral dimension of a lens designed for ultrasonic frequencies. Labyrinthine structures have been used by different authors^{12–16} to achieve a lensing effect by directly sculpting the phase of an impinging wavefront. Cavity structures have been developed to design a lens by the same units to avoid complex fabrication.¹⁷ In all these cases, however, 3D structures are needed to focus acoustic waves in three dimensions, and the geometries are, therefore, so intricate that scaling-up manufacturing is highly challenging.¹⁸

Sonic crystals (“SCs”)¹⁹ are a special type of metamaterials, characterized by the periodic arrangement of the same unit cell, scaled and arranged into a background material (like air or water). Typically manufactured by extrusion of 2D structures, sonic crystals have been successfully used to achieve phenomena such as anomalous refraction,^{20,21} acoustic cloaking,²² and wave guiding.²³ Sonic crystals have also successfully been used to achieve lensing in 2D, using the “homogenization method” to obtain a locally variable refractive index by filling fractions of unit cells.^{24–27} Furthermore, this method was optimized to achieve invariant focal length with broadband frequency.²⁸ Very recently, 3D sound focusing using a 2D periodic structure has been demonstrated underwater at ultrasonic frequencies,^{29,30} but there are not many studies on achieving 3D acoustic convergence through 2D sonic structures in air.

In this paper, we show how an extruded 2D hexagonal lattice array of rigid cylinders with gradient diameters can be used to focus

audible sound in air in three dimensions. This device we have called a 2.5D lens. We demonstrate the validity of this approach by simulating and measuring the pressure behind two lenses, designed for 8 kHz: one with a focal length of 1.6λ and a “super-lens,” whose focal distance is smaller than the wavelength λ of the incident wave. These lenses will also contribute to potential applications, like acoustic contactless power transfer.^{31–33}

We first utilize the gradient index theory from optics³⁴ to determine which variation of the effective refractive index is needed across the lateral dimension of a lens to achieve 2D focusing (i.e., in the xy -plane). Without loss of generality, we will focus our discussion to the case of sonic crystals made by cylinders of different diameters (see Fig. 1), designed for operation at 8 kHz ($\lambda \approx 4.3$ cm).

To describe sonic crystals with an effective refractive index, like in optics, the dimension of sonic crystals should be sub-wavelength. We, therefore, consider each cylinder inserted into a hexagonal unit cell and assume that a , the lattice constant, is much smaller than wavelength of the incident wave. Here, we adopt an 8 kHz incident plane wave and let $a = 1$ cm.

Then, we select a hyperbolic secant profile for the effective refractive index.²⁷ The effective refractive index $n(y)$ is, therefore, defined as

$$n(y) = n_0 \operatorname{sech}(\alpha y), \quad (1)$$

where α is a gradient coefficient, defined as

$$\alpha = \frac{1}{h} \cosh^{-1} \frac{n_0}{n_h}, \quad (2)$$

with h is the half the height of the lens, n_h is the refractive index at the edges of the lens, and n_0 is the refractive index in the middle of the lens (i.e., at $y=0$). Based on this given profile, the ray trajectory of acoustic beams is determined by

$$y(x) = \frac{1}{\alpha} \sinh^{-1}(u_0 H_f(x)), \quad (3)$$

where $u_0 = \sinh(\alpha y_0)$ and $H_f(x) = \cos(\alpha x)$. By following this equation and Snell's law, it is easy to calculate the position of the focal spot (see the [supplementary material](#)) given the thickness of the lens and its lateral dimension.

For the first example in this paper, we assume $n_0 = 1.3$ and $n_h = 1$ and utilize seven layers of cylinders along the x -axis for a thickness in the direction of propagation $d = 6.4$ cm and six layers along the y -axis, which means a half height equal to $h = 6a$. According to our calculations based on the gradient index theory, the focal position is placed at 7.2 cm (see the [supplementary material](#), Sec. S1).

Once the desired value is determined at each point, the effective refractive index of each unit cell is achieved by varying its filling fraction, so that $n = \sqrt{1+f}$, where $f = 2\pi/\sqrt{3}(R/a)^2$ is decided by radius of the cylinder.³⁵

To explain convergence in the xz -plane, we start by calculating the band structures for unit cells with different cylinder diameters: those relative to the largest and smallest diameters are illustrated in Fig. 2.

The solid/dashed lines show the dispersion relation of unit cells made by cylinders with the largest/smallest diameter, and the black line is the incident wave with 8 kHz. Given that we used the largest and the smallest cylinders, we infer that a 8 kHz incident wave can pass through all the cylinders in the xy -plane.

To expand this result to the xz -plane, we treat all cylinders as 3D sonic crystals, each constituted by nine shorter cylinders stacked together with the height of each shorter cylinder equal to the lattice constant of the hexagonal unit cell ($a = 1$ cm). The 3D equifrequency contours (EFCs) of the cylinders with the largest diameter (and 1 cm height) are then calculated in COMSOL and shown in Fig. 3(a) for the

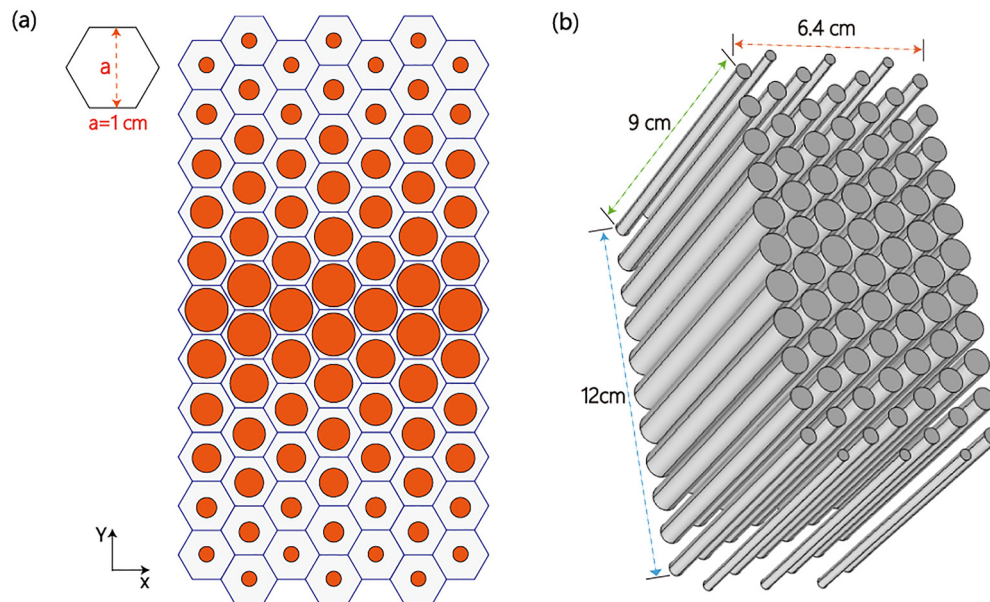


FIG. 1. Schematic representation of the sonic crystals used in this study: (a) cross section of the cylinders inside the hexagonal lattice along the xy -plane; (b) 3D view of the 2.5D gradient index lens.

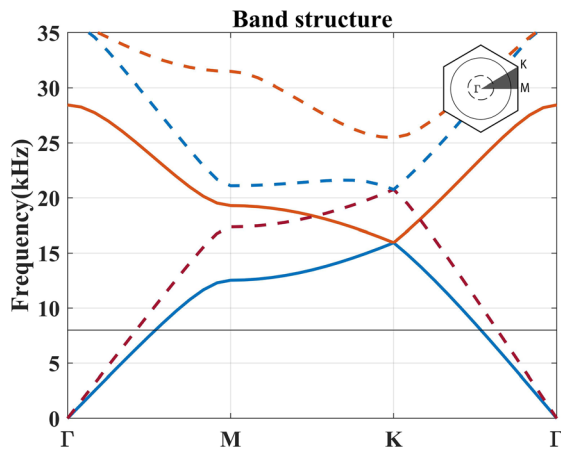


FIG. 2. Band structure of the hexagonal lattice with the largest cylinder (solid line) and the smallest cylinder (dashed line).

plane $y = 0$ (which contains the axis of the cylinder). It is observed that the EFCs for frequencies between 5 and 10 kHz are elliptic and anisotropic along the x -axis, and this results in focusing in the xz -plane. To explain this phenomenon, we present in Fig. 3(b) the EFCs of the largest cylinders (black ellipse) and of free space (blue dashed circle) at 8 kHz in the xz -plane. Also in Fig. 3(b) are shown the incident wave vector k_i (red arrow), the refracted wave vectors k_r (blue arrows), and the group velocity v_g (green arrows). As expected, the group velocity, which is the direction of energy transport, is perpendicular to the EFCs.

When the 8 kHz incident wave (red arrow) hits the sonic crystal made with the largest cylinders, the energy is decomposed into two directions (green arrows) at the interface between air and sonic crystals (black dashed line), and a large part of energy focuses toward the x -axis due to the symmetric refraction. At the center of a lens like the one in Fig. 1, focusing is expected in the xz -plane.

Since the diameter of the cylinders changes along y , it is worth looking at what happens at the end of the lens. To this aim, we calculated the EFCs of the smallest cylinders in the xz -plane [Fig. 4(a)] and compared them with the EFC of the free space at 8 kHz [Fig. 4(b)]. It can be observed that the EFC of the periodic structure containing only the smallest cylinders is similar to the EFC of the free space: the smallest cylinders, therefore, have a lower focusing capability (i.e., a longer focal length). Therefore, a plane wave entering our lens in the x direction will experience a focusing, which is not the same along y , since the converging power of the cylinders in the xz -plane depends on their diameter.

To verify the phenomenon, we used COMSOL5.4(a) to run numerical simulations in the xy -plane and in the xz -plane [Figs. 5(a) and 5(b)]. The simulation area in the xy -plane was $20 \times 12 \times 10 \text{ cm}^3$ behind the lens.

In Fig. 5(a), a plane wave with 8 kHz propagates from left to right, and the simulated acoustic intensity shows a clear maximum in the pressure distribution after it passes through the lens, both in the xy -plane and the xz -plane. We call this effect 2.5D focusing. It is worth noting that not only the maximum is located approximately at 65 mm from the lens, as expected from the theory, but also that focusing is

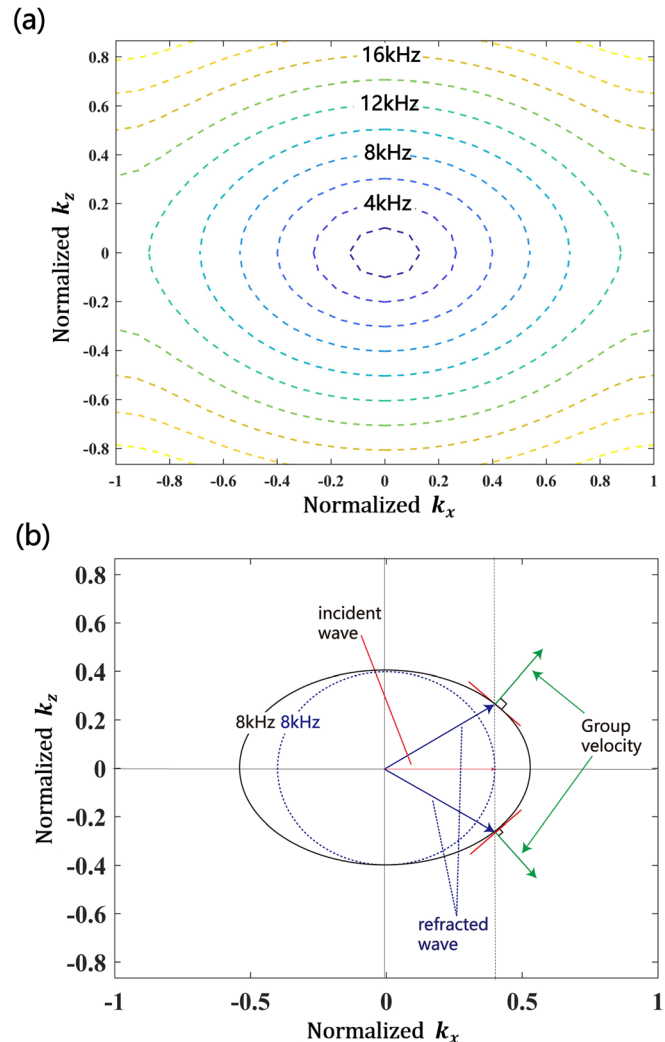


FIG. 3. (a) The EFCs of the cell with the largest cylinders in the xz -plane, and k_x and k_z are normalized wave vectors along the x -axis and the z -axis, respectively. (b) The incident wave vector k_i is indicated by the red arrow. The refracted wave vector k_r and group velocity v_g are indicated by blue and green arrows, respectively.

limited to the central part of the lens, since the smallest cylinders contribute less to the effect. In the measurements (see below), it will, therefore, be crucial to limit the amount of energy passing along the sides of the lens.

One of the key successes of metamaterials is the ability to focus at distances smaller than the wavelength but very close to the Rayleigh diffraction limit (“super-lens”). To prove that our approach could also be used for this type of device, we realized another 2.5D lens using the cylinders with same diameters but ten layers along the x -axis. By numerical simulations in Figs. 6(a) and 6(b), we achieved 2.5D focusing at a distance of 3.7 cm from the lens, while the focal length of calculation based on Eq. (3) is 3.1 cm (see the supplementary material, Sec. S1).

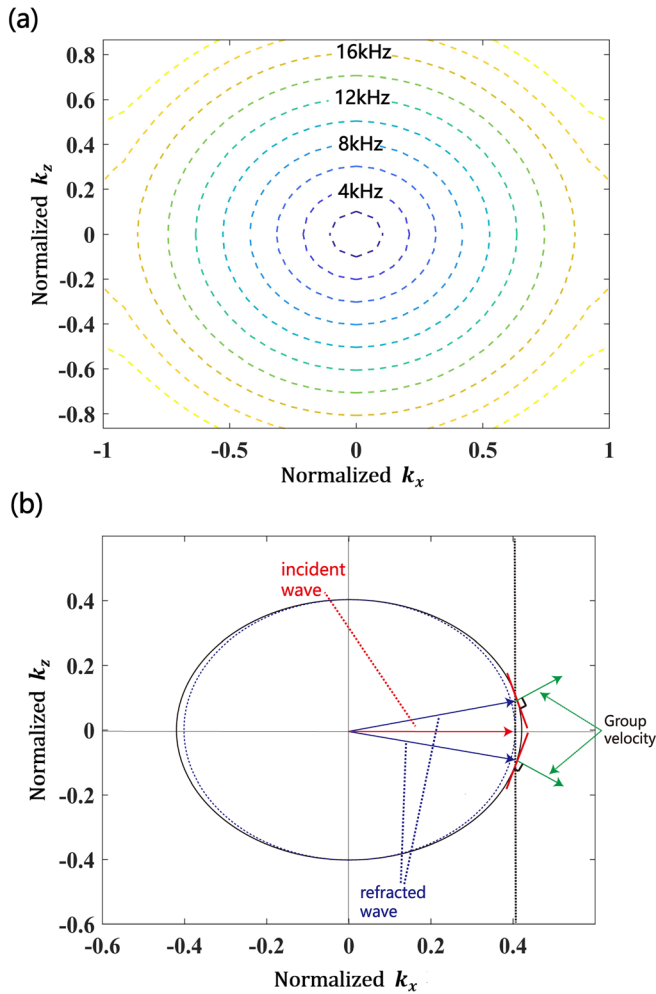


FIG. 4. (a) The EFCs of the cell with the smallest cylinders in the xz -plane, and k_x and k_z are normalized wave vectors along the x -axis and the z -axis, respectively. (b) The incident wave vector k_i is indicated by the red arrow. The refracted wave vector k_r and group velocity v_g are indicated by blue and green arrows, respectively.

To experimentally validate the performance of the 2.5D lenses, we conducted quantitative measurements of the acoustic field behind them. The experimental setup is shown in Fig. 7(a). A function/arbitrary waveform generator (RSDG 2042X) was amplified and connected to a JVC loudspeaker (JVC CS J520X) to produce an 8 kHz sine wave. The source-amplifier-loudspeaker system was found to have a flat response in frequency in the range of interest (6–10 kHz) in previous experiments. The loudspeaker’s emission was channeled into a plastic cylindrical waveguide with similar diameter, while the 2.5D lens being tested was placed to the other side of the waveguide. The length of the waveguide (27 cm) was sufficiently long for the emission to have developed a planar wavefront before reaching the 2.5D lens. Since the theory indicated that we should minimize the sound hitting the sides of the lens, a black commercial absorber was used to shape the exit of the

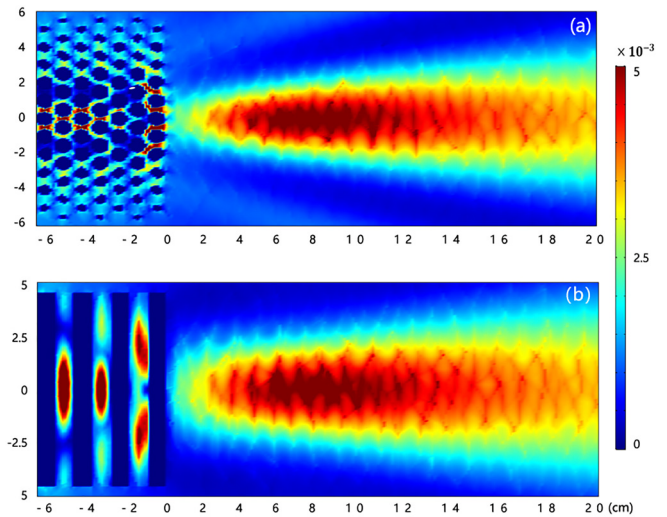


FIG. 5. (a) Acoustic intensity of 2.5D lens at 8 kHz in the xy -plane; (b) Acoustic intensity of 2.5D lens at 8 kHz in the xz -plane.

waveguide and ensure a better coupling to the lens in the yz -plane in Fig. 7(b). This solution was preferred to inserting the lens inside the waveguide, as the latter solution would have enhanced the energy hitting the sides of the lens.

In our experiments, each experiment of the x -axis was repeated 13 times to get more precise results on the location of the focal point, and each experiment of the y -axis and the z -axis was repeated six times, in order to obtain for each selected measuring position a statistically relevant mean and standard deviation.

It is worth noting that, before comparing these measurements with simulations, the COMSOL model had to be adjusted to include the waveguide (see the supplementary material). Particularly

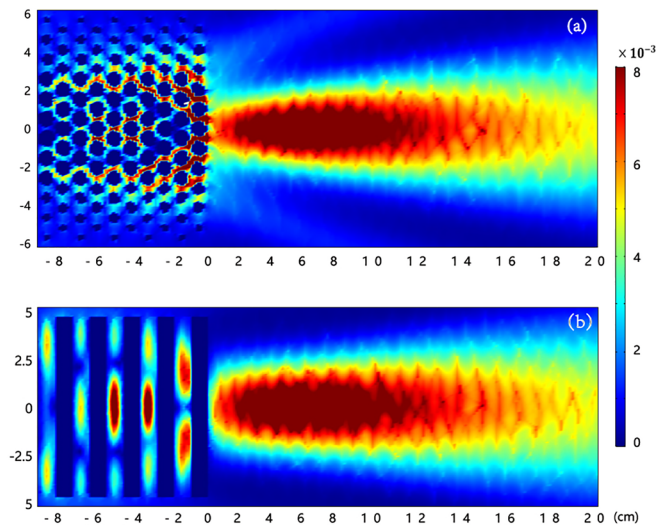


FIG. 6. (a) Acoustic intensity of super lens at 8 kHz in the xy -plane; (b) Acoustic intensity of super lens at 8 kHz in the xz -plane.

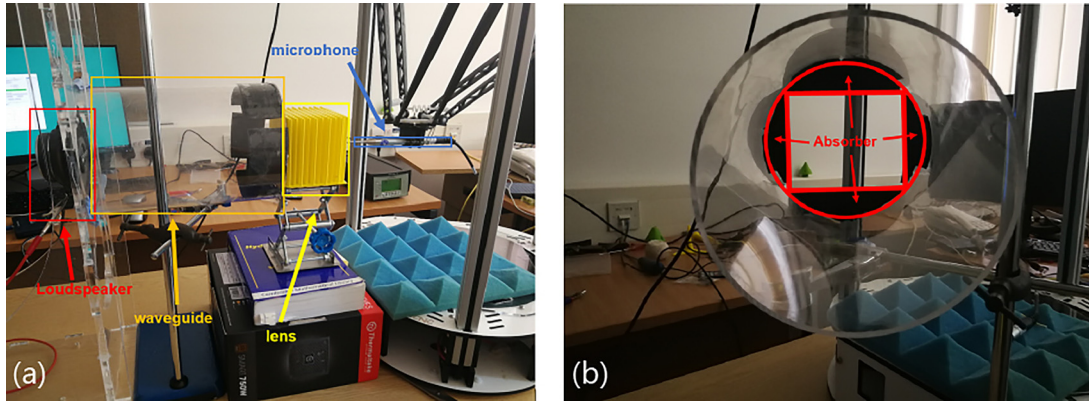


FIG. 7. (a) Experimental setup with the waveguide highlighted. (b) The exit of the waveguide, shaped to match the lens in the yz -plane.

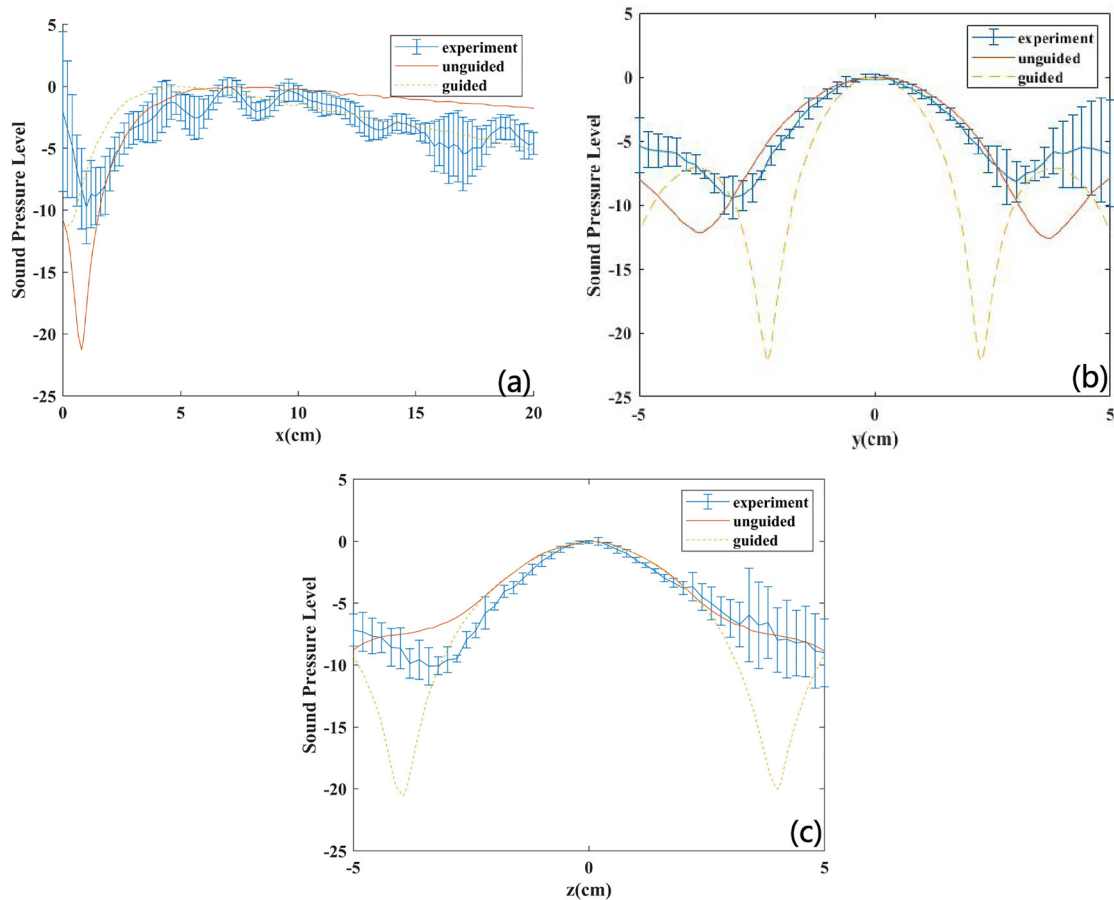


FIG. 8. (a) Sound pressure level (dB) distributions behind the lens with seven layers along the x -axis. The highest point is at $x = 75$ mm in unguided simulation while in guided simulation, the highest point is at $x = 46$ mm. In the experiments, the highest point was at $x = 72 \pm 2$ mm. (b) Sound pressure level (dB) distributions along the y -axis in unguided simulation, guided simulation, and experimental result. (c) Sound pressure level (dB) distributions along the z -axis in unguided simulation, guided simulation, and experimental result.

challenging was simulating the coupling between the waveguide and the lens, and therefore, Figs. 8 and 9 present two simulations:

- Unguided condition simulation (red solid line), where the absorbing material was simulated with a perfectly matched layer (totally absorbing), and the lens is basically in a free space, surrounded by perfectly matched layers. This simulation is, therefore, physically similar to the one used for Figs. 5 and 6.
- Guided simulation (yellow dashed line). In this case, the coupling material is treated as a reflective solid, thus eliminating diffraction along the sides: the lens behaves as if partially immersed in the waveguide.

Other attempt to simplify the coupling between the guide and the lens (e.g., 3D-printing a coupler, as the one described in the [supplementary material](#)) ended with similar results.

In Fig. 8, we compare the measured sound pressure levels with the simulations for the 72 mm lens. First, we measured pressure along a central line in the x -direction [see Fig. 8(a)] in the region between 2 and 200 mm behind the lens and noted that the position with the highest value was at $x = 72 \pm 2$ mm from the lens. We also observe

that, while the highest pressure is at $x = 75$ mm in the unguided simulation, the maximum moves to $x = 46$ mm in the guided simulation. Figure 8(a) also shows that, the experimental result along the x -axis has similar trend with the unguided simulation in the initial curve, while appears closer to the guided case in the latter part.

The position of the highest pressure was then used as the central point for the scans/simulations in the other directions, along y [Fig. 8(b)] and along z [Fig. 8(c)], both from -50 to 50 mm.

We observe that, while along the y -axis the experimental result is located between the two simulations, almost no effect of the coupling material can be seen in z , where the cylinders were closed by horizontal plates. This result illustrates that the diffraction at the edges is the main reason causing differences between simulations and experimental results. Also visible (from the scans along y and z) is a limitation of our oscilloscope that could only acquire a dynamical range of 12 dB. While not discussed here, the role of thermo-viscous effects was found to be minimal in previous studies.

We, therefore, attribute the other differences between numerical simulations and experimental results in Fig. 8 to the 3D-printing process (which left the surface of the smallest cylinders particularly

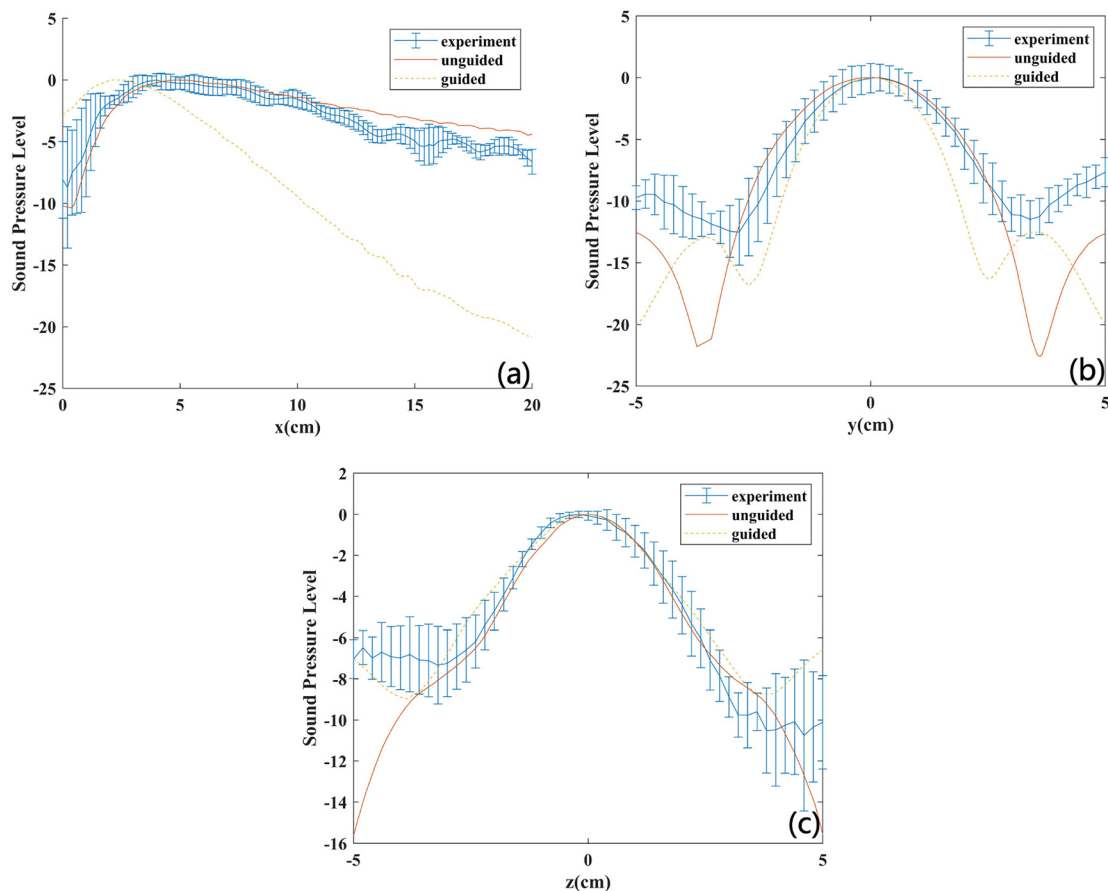


FIG. 9. (a) Sound pressure level (dB) distributions behind the super lens with ten layers along the x -axis. The highest point is at $x = 49$ mm in unguided simulation while in guided simulation, the highest point is at $x = 22$ mm. In experiments, the highest point was at $x = 42 \pm 2$ cm. (b) Sound pressure level (dB) distributions along the y -axis in unguided simulation, guided simulation, and experimental result. (c) Sound pressure level (dB) distributions along the z -axis in unguided simulation, guided simulation, and experimental result.

rough), to difficulties in aligning the lens with the speaker [e.g., the asymmetry of the side lobes in Fig. 8(c)], and to differences in the values of the material parameters between simulations and experiments.

The results relative to the ten layers super-lens can be found in Fig. 9, which shows a comparison between measured sound pressure levels and the two simulations (“guided” and “unguided”) along the x -axis, the y -axis, and the z -axis. The focal distance of the unguided simulation is at $x = 49$ mm, while that of the guided simulation is at $x = 22$ mm. In this case, the position of the measured maximum is at 42 ± 2 mm. While similar considerations to the ones made for the first lens can be taken into Fig. 9(b) (y -axis) and to Fig. 9(c) (z -axis), the behavior along the x -axis strongly depends on the type of simulation both close to the lens and in the far field. In this case, the unguided curve appears closer to the measurements, while the measurements in the near and far field appear between the two cases. It is worth noting that, since our experiments were conducted in a room, we used a waveguide both to ensure a planar wavefront at the input side of our lens and to minimize the energy lost in scattering (from the borders of the lens) and in reflections (from other objects). In practical applications, the same conditions can be achieved by placing the source sufficiently far away from the lens and by removing unwanted reflections (e.g., in the free space or using absorbing materials).

In this paper, we have demonstrated that an extruded 2D array of cylinders with graded diameter can be used as a 2.5D metamaterial lens, enabling to focus sound in three dimensions. This has been achieved using the gradient index theory to realize sound focusing in the horizontal plane (i.e., the xy -plane), while band structures and equifrequency contours were utilized to explain acoustic focusing in the xz -plane. We have demonstrated the feasibility of our design procedure first with finite-element simulations and then with measurements, testing it on two lenses, one with a focal length greater than the wavelength and one with a focal length smaller than the wavelength. Testing and simulations were done at a single frequency, 8 kHz.

These types of lenses, due to their easy fabrication, provide a simple way to manipulate sound in air. Future work will look at the potential of using these geometries to correct loudspeaker divergence and to achieve an adjustable focal distance. Equally important for applications (e.g., directional sound, acoustic collimator) is the bandwidth of these devices, so testing at other frequencies close to 8 kHz will be highly desirable, as will be the use on non-cylindrical geometries, capable of achieving the same result over larger bandwidths.

See the [supplementary material](#) for the complete process of calculating focal length, description of boundary conditions used in the simulations, explanation of the relationship between equifrequency contours and focal capability, fabrication of lenses and data processing, and comparison between the GRIN lens and the convex lens.

Yuanyan Zhao was supported by the School of Engineering and Informatics in the University of Sussex. Professor Sriram Subramanian’s contribution was supported by the EU-H2020 through their ERC Advanced Grant (No. 787413) and the Royal Academy of Engineering through their Chairs in Emerging Technology Program (No. CIET18/19). Dr. Gianluca Memoli was supported by the Engineering and Physical Sciences Research Council (EPSRC-UKRI) through Grant No. EP/S001832/1 “AURORA: Controlling sound like we do with light.”

DATA AVAILABILITY

The data that support the findings of this study are available from the corresponding author upon reasonable request.

REFERENCES

- J. Li and C. T. Chan, “Double-negative acoustic metamaterial,” *Phys. Rev. E* **70**, 055602(R) (2004).
- S. A. Cummer, J. Christensen, and A. Alù, “Controlling sound with acoustic metamaterials,” *Nat. Rev. Mater.* **1**, 1–14 (2016).
- B. Assouar, B. Liang, Y. Wu, Y. Li, J. C. Cheng, and Y. Jing, “Acoustic metasurfaces,” *Nat. Rev. Mater.* **3**, 460–472 (2018).
- B. I. Popa, L. Zigoneanu, and S. A. Cummer, “Experimental acoustic ground cloak in air,” *Phys. Rev. Lett.* **106**, 253901 (2011).
- B. I. Popa and S. A. Cummer, “Homogeneous and compact acoustic ground cloaks,” *Phys. Rev. B* **83**, 224304 (2011).
- Y. Xie, C. Shen, W. Wang, J. Li, D. Suo, B. I. Popa, Y. Jing, and S. A. Cummer, “Acoustic holographic rendering with two-dimensional metamaterial-based passive phased array,” *Sci. Rep.* **6**, 35437 (2016).
- S. Zhang, C. Xia, and N. Fang, “Broadband acoustic cloak for ultrasound waves,” *Phys. Rev. Lett.* **106**(2), 1–4 (2011).
- V. Fokin, M. Ambati, C. Sun, and X. Zhang, “Method for retrieving effective properties of locally resonant acoustic metamaterials,” *Phys. Rev. B* **76**, 144302 (2007).
- B. I. Popa and S. A. Cummer, “Design and characterization of broadband acoustic composite metamaterials,” *Phys. Rev. B* **80**, 174303 (2009).
- L. Zigoneanu, B. I. Popa, and S. A. Cummer, “Design and measurements of a broadband two-dimensional acoustic lens,” *Phys. Rev. B* **84**, 024305 (2011).
- Y. Jin, R. Kumar, O. Poncelet, O. Mondain-monval, and T. Brunet, “Flat acoustics with soft gradient-index metasurfaces,” *Nat. Commun.* **10**, 143 (2019).
- G. Memoli, M. Caleap, M. Asakawa, D. R. Sahoo, B. W. Drinkwater, and S. Subramanian, “Metamaterial bricks and quantization of meta-surfaces,” *Nat. Commun.* **8**, 14608 (2017).
- M. A. Norasikin, D. Martinez Plasencia, S. Polychronopoulos, G. Memoli, Y. Tokuda, and S. Subramanian, “SoundBender: Dynamic acoustic control behind obstacles,” in The 31st Annual ACM Symposium on User Interface Software and Technology—UIST ’18 (2018), pp. 247–259.
- G. Memoli, L. Chisari, J. P. Eccles, M. Caleap, B. W. Drinkwater, and S. Subramanian, “Vari-Sound: A varifocal lens for sound,” in *Conference on Human Factors in Computing Systems - Proceedings* (ACM, 2019), pp. 1–14.
- Y. Li and M. B. Assouar, “Three-dimensional collimated self-accelerating beam through acoustic metascreen,” *Sci. Rep.* **5**, 17612 (2015).
- R. Ghaffarivardavagh, J. Nikolajczyk, R. G. Holt, S. Anderson, and X. Zhang, “Horn-like space-coiling metamaterials toward simultaneous phase and amplitude modulation,” *Nat. Commun.* **9**, 1349 (2018).
- J. Qian, J. P. Xia, H. X. Sun, S. Q. Yuan, Y. Ge, and X. Z. Yu, “Broadband acoustic focusing by cavity structures with phase manipulations,” *J. Appl. Phys.* **122**, 244501 (2017).
- Y. Xie, Y. Fu, Z. Jia, J. Li, C. Shen, Y. Xu, H. Chen, and S. A. Cummer, “Acoustic imaging with metamaterial Luneburg lenses,” *Sci. Rep.* **8**, 16188 (2018).
- A. Gupta, “A review on sonic crystal, its applications and numerical analysis techniques,” *Acoust. Phys.* **60**, 223–234 (2014).
- M. Ke, Z. Liu, C. Qiu, W. Wang, J. Shi, W. Wen, and P. Sheng, “Negative-refraction imaging with two-dimensional phononic crystals,” *Phys. Rev. B* **72**, 064306 (2005).
- S. Yang, J. H. Page, Z. Liu, M. L. Cowan, C. T. Chan, and P. Sheng, “Focusing of sound in a 3D phononic crystal,” *Phys. Rev. Lett.* **93**, 024301 (2004).
- V. M. García-Chocano, L. Sanchis, A. Díaz-Rubio, J. Martínez-Pastor, F. Cervera, R. Llopis-Pontiveros, and J. Sánchez-Dehesa, “Acoustic cloak for airborne sound by inverse design,” *Appl. Phys. Lett.* **99**, 074102 (2011).
- L. Y. Wu and L. W. Chen, “An acoustic bending waveguide designed by graded sonic crystals,” *J. Appl. Phys.* **110**, 114507 (2011).
- D. Torrent and J. Sánchez-Dehesa, “Acoustic metamaterials for new two-dimensional sonic devices,” *New J. Phys.* **9**, 323 (2007).
- T. P. Martin, M. Nicholas, G. J. Orris, L.-W. Cai, D. Torrent, and J. Sánchez-Dehesa, “Sonic gradient index lens for aqueous applications,” *Appl. Phys. Lett.* **97**, 113503 (2010).

- ²⁶A. Climente, D. Torrent, and J. Sánchez-Dehesa, “Sound focusing by gradient index sonic lenses,” *Appl. Phys. Lett.* **97**, 104103 (2010).
- ²⁷S. C. S. Lin, T. J. Huang, J. H. Sun, and T. T. Wu, “Gradient-index phononic crystals,” *Phys. Rev. B* **79**, 094302 (2009).
- ²⁸J. Hyun, W.-H. Cho, C.-S. Park, J. Chang, and M. Kim, “Achromatic acoustic gradient-index phononic crystal lens for broadband focusing,” *Appl. Phys. Lett.* **116**, 234102 (2020).
- ²⁹Y. Ruan, X. Liang, Z. Wang, T. Wang, Y. Deng, F. Qu, and J. Zhang, “3-D underwater acoustic wave focusing by periodic structure,” *Appl. Phys. Lett.* **114**, 081908 (2019).
- ³⁰H. Sun, S. Wang, S. Huang, L. Peng, Q. Wang, and W. Zhao, “Design and characterization of an acoustic composite lens with high-intensity and directionally controllable focusing,” *Sci. Rep.* **10**, 1469 (2020).
- ³¹M. Roes, M. Hendrix, and J. Duarte, “Contactless energy transfer through air by means of ultrasound,” in *IECON 2011-37th Annual Conference of the IEEE Industrial Electronics Society* (IEEE, 2011), pp. 1238–1243.
- ³²M. G. Roes, J. L. Duarte, M. A. Hendrix, and E. A. Lomonova, “Acoustic energy transfer: A review,” *IEEE Trans. Ind. Electron.* **60**, 242–248 (2013).
- ³³V. F.-G. Tseng, S. S. Bedair, and N. Lazarus, “Phased array focusing for acoustic wireless power transfer,” *IEEE Trans. Ultrason., Ferroelectr., Frequency Control* **65**, 39–49 (2018).
- ³⁴C. Gomez-Reino, M. Perez, and C. Bao, *Gradient-Index Optics: Fundamentals and Applications* (Springer, 2002), p. 241.
- ³⁵F. Cervera, L. Sanchis, J. V. Sánchez-Pérez, R. Martínez-Sala, C. Rubio, F. Meseguer, C. López, D. Caballero, and J. Sánchez-Dehesa, “Refractive acoustic devices for airborne sound,” *Phys. Rev. Lett.* **88**, 023902 (2001).